Porosity dependence of electron percolation in nanoporous TiO_2 layers

Ashi Ofir,[1] Snir Dor,[1] Larisa Grinis,[1] Arie Zaban,[1] Thomas Dittrich,[2] and Juan Bisquert[3,a)]
[1]*Department of Chemistry, Nano-Energy Center, Bar-Ilan University, Ramat-Gan 52900, Israel*
[2]*Hahn-Meitner-Institute, Glienicker Str. 100, D-14109 Berlin, Germany*
[3]*Departament de Física, Universitat Jaume I, 12071 Castelló, Spain*

(Received 1 October 2007; accepted 4 January 2008; published online 11 February 2008)

The electron diffusion coefficient at varying porosity has been determined in a series of nanostructured TiO_2 films of different initial thicknesses. The porosity was changed by applying different pressures prior to sintering, thereby modifying the internal morphology of the films though not their chemical and surface conditions. A systematic increase of the effective diffusion coefficient was observed as the porosity was decreased, indicating the improvement of the internal connectivity of the network of nanoparticles. The experimental results have been rationalized using percolation theory. First of all, applying a power law dependence, the diffusion coefficient as a function of porosity from different films collapsed in a single master curve. In addition, application of the models of effective medium approximation (EMA) allows us to compare the experimental results with previous data from Monte Carlo simulation. The different data show a similar dependence in agreement with the EMA predictions, indicating that the geometrical effect of electron transport due to variation of porous morphology in TiO_2 nanoparticulate networks is well described by the percolation concept. © *2008 American Institute of Physics*. [DOI: 10.1063/1.2837807]

INTRODUCTION

Nanostructured metal oxide films formed by interconnected nanoparticles provide a large internal area that can realize different functionalities. The semiconductor particles, prepared by wet chemical methods, are usually deposited by screen printing, onto a glass or flexible plastic support covered with a conducting layer. The film is thermally treated to form an electronically connected mesoporous array, which is filled with an ionic conductor or hole-conducting medium. Such metal oxide nanostructures (e.g., TiO_2, ZnO, SnO_2, and Nb_2O_5) are well suited for cheap large-scale production of devices and have been investigated for several applications such as dye-sensitized solar cells (DSCs),[1] photoelectrochromic windows,[2] electrical paint displays,[3] and protein immobilization.[4]

A major factor in the operation of metal oxide nanostructured films is the efficient electronic communication between the conducting substrate and the internal surface of the film. Electron transport in the nanoparticle network ensures that the whole functionalized surface is addressable from the contacts. Therefore, electron transport in nanostructured metal oxides has been the subject of numerous investigations.[5–9] Often, metal oxide nanoparticles are natively insulating, but they obtain a large conductivity by electrically injected or photoinduced charge carriers. Long range electrical fields are shielded by ionic charge in the electrolyte, and electron transport occurs by diffusion in the majority of instances.[10] It has been widely reported that electron displacement is a trap-limited process, which explains the variations of the diffusion coefficient as a function of steady-state conditions (S) and temperature.[11,12] Analysis of the effects of traps on electron transport usually employs a macrohomogeneous model, in which the chemical diffusion of electron coefficient takes the form[13]

$$D_n = F(S)D_{\mathrm{cb}}, \tag{1}$$

where D_{cb} is the diffusion coefficient of free electrons in extended states (conduction band) and F is a factor related to trapping-detrapping events. Another issue of recent interest is the specific effect of the geometry of the nanoparticulate array on the macroscopic transport.[14–19] Van de Lagemaat and co-workers first considered the relation between particle coordination number and porosity in TiO_2 nanoparticulate films and described macroscopic transport in terms of the percolation model.[14,15] Other authors have considered the variations of the network morphology[16,17] and the influence of such morphology on the performance of DSC.[18]

One accurate method to measure the diffusion coefficient is the transient photocurrent measurements.[10] A typical diffusion peak is usually observed for strong excitation from the electrolyte side, corresponding to the diffusion of electrons from the outer edge of the nanocrystalline film to the collecting substrate, along the layer thickness L, as indicated in Fig. 1(a). For nondispersive transport, the measured effective diffusion coefficient (D_{eff}) can be obtained from the time at the maximum of the diffusion photocurrent (t_{peak}),

$$D_{\mathrm{eff}} = \frac{L^2}{6t_{\mathrm{peak}}}. \tag{2}$$

It should be noted that t_{peak} should be less or of the same order as the lifetime of the diffusing excess carrier.[20] Figure 1(b) gives a two-dimensional schematic for percolation paths of a charge carrier in a porous network with two different porosities. For lower porosity, the number of possible percolation paths increases due to an increasing average coordina-

a)Electronic mail: bisquert@fca.uji.es.

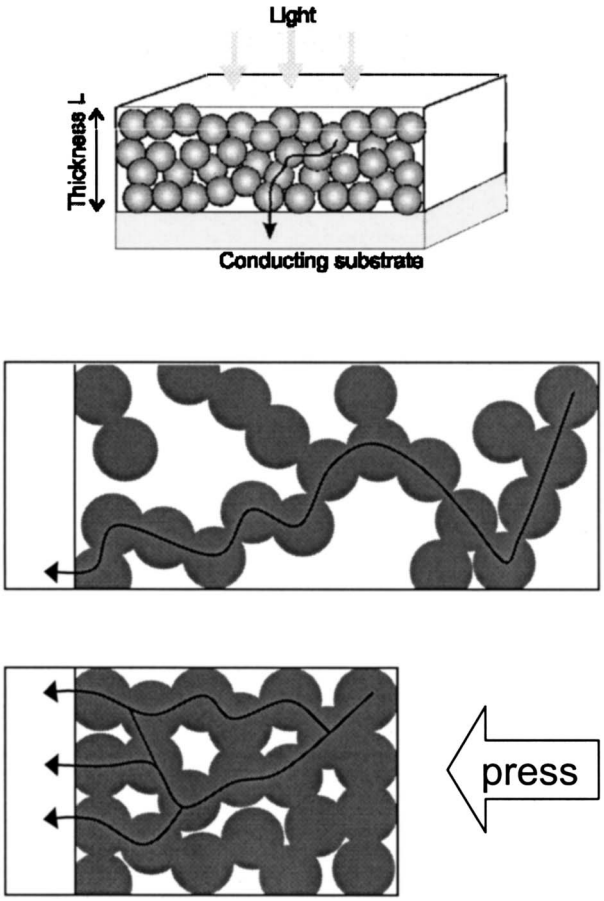

FIG. 1. Schematic of changing percolation paths of unpressed (upper) and pressed (lower) porous electrodes due to decrease of porosity.

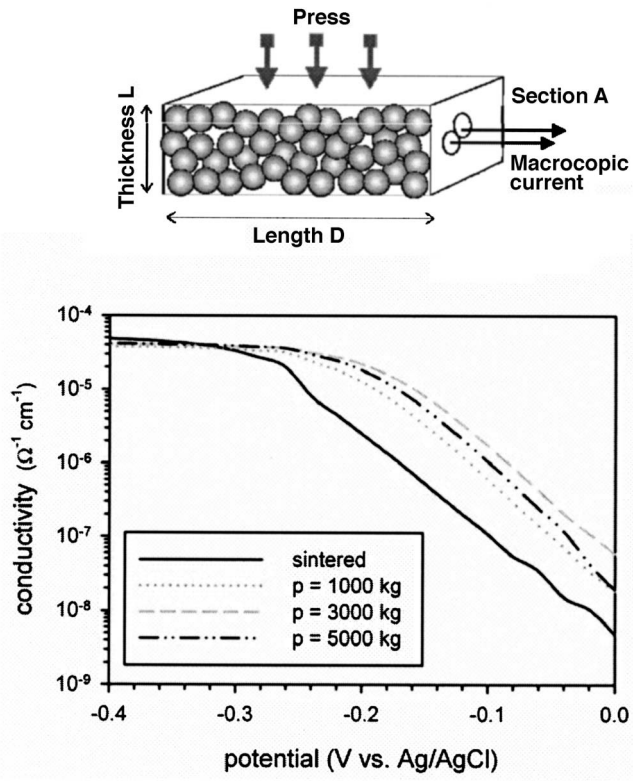

FIG. 2. Electronic conductivity of a set of nanoparticulate TiO_2 electrodes compressed at different pressures as indicated. The starting thickness of the films is similar in all cases, and all films were sintered after pressing. The conductivity is determined from the current between parallel contacts (Ref. 9), normalizing to the length, width, and thickness of the TiO_2 layer. The original thickness before pressure L is taken in all the cases, since there is no change in the amount of TiO_2 present on the electrode.

tion number of particles. By this way, there are less "dead ends," the length of the percolation paths decreases, and therefore, the transport through the layer becomes faster.

It follows that the effective diffusion coefficient of electrons contains a geometric factor D_g due to the film morphology in addition to the value of Eq. (1); the latter can be considered as an upper limit for diffusive transport at zero porosity,

$$D_{\text{eff}} = D_g F(S) D_{\text{cb}}. \tag{3}$$

Further understanding of the relation of the geometric factor D_g to sample morphology (i.e., number of interconnects between the nanoparticles) and porosity of disordered nanoparticulate TiO_2 networks is important, for both practical and fundamental aspects. These electrodes provide a high performance in DSC, and long range transport of electrons may have an effect on recombination processes.[21] It should enable comparison with the properties of highly ordered geometries such as nanotube arrays.[22] Finally, the analysis of D_g poses an interesting problem of percolation conduction in disordered media.[23]

Studying the D_g in isolation is not straightforward, since variations of the samples may affect the other factors in Eq. (3) as well. In recent works, a unique model system of nanoporous TiO_2 prepared by electrophoretic deposition (EPD) technique has been reported.[19,24] For this system, a systematic change of the porosity is possible, reducing the thickness L of the film by pressing of deposited electrodes (in the direction normal to the substrate) at different pressures. During pressing, the TiO_2 nanoparticles can freely change their positions relatively to each other since they are not yet fixed to each other after EPD. The positions of the TiO_2 nanoparticles will be fixed only after pressing by sintering at high temperature. In addition, the sintering process is responsible for the conditioning of the internal TiO_2 surfaces giving equal boundary to the electrolyte for all samples.

As a qualitative illustration of the changes of transport properties under progressive compactification of the electrodes, Fig. 2 shows the results of electron conductivity of a series of pressed (and sintered) nanostructured TiO_2 electrodes that were measured in electrochemical transistor configuration.[9] Note that this measurement is different from that indicated in Fig. 1(a). Here, as indicated in Fig. 2, the film is deposited over an insulating gap in the conductive substrate; therefore, in this case, the conductance, i.e., current versus voltage, G, is measured in the direction parallel to the substrate. The conductivity σ relates to the measured conductance as $\sigma = DG/A$, where D is the film length and A is the section. The results in Fig. 2 show that the conductivity *increases* as the film becomes thinner, i.e., as the geometric cross section of the film decreases. This is because the TiO_2 particles are nearly incompressible, so that under pressing, the spheres rearrange themselves to reduce the void volume. Therefore, the cross section of TiO_2 *material* remains the

same as the films become thinner. Meanwhile, the connectivity between the nanoparticles improves, which explains the observed increase of the conductance in Fig. 2. Hereafter, all the results reported refer to the configuration of Fig. 1.

In this work, the transport properties of a set of different TiO_2 porous electrodes with varying porosities are reported. With respect to previous works,[19,24] a much larger set of experimental results has been obtained (see below, Fig. 7) that allows for a more systematic investigation. The information obtained on the geometric component of the electron diffusion coefficient is interpreted in the light of percolation concepts. It is important to observe that the porosities of nanostructured TiO_2 films, (sintered films prepared by the hydrothermal method) may not be close to the percolation limit, which requires a rather open structure. Therefore, here, we adopt an extended view in which not only the region close to but also that far from the critical concentration of the nanoparticulate network is considered. Our main aim is to show that the geometrical effect of electron transport due to variation of porous morphology in TiO_2 nanoparticulate networks is well described by the percolation theory. In particular, we make use of the effective medium approximation (EMA), which is a method known to describe well percolation transport well above the critical concentration.[23] This approach effectively broadens the interpretation of the geometrical features of electron transport in nanostructured semiconductors.

EXPERIMENTAL

Nanoporous TiO_2 electrodes were prepared on fluorine doped tin oxide substrates (glass coated with conductive SnO_2:F) by EPD of TiO_2 nanoparticles (P25). The EPD was performed in organic solution at moderate potential. The initial layer thicknesses were varied by changing the deposition time. The layer thicknesses were measured with a step profiler. The thicknesses of the unpressed electrodes were 14.9, 14.5, 8.1, 5.4, and 3.5 μm. An advantage of the EPD technique is that the porosity is independent of the layer thickness.

After EPD, four samples were separated for each initial thickness and pressed at 200, 400, 600, and 800 kg/cm^2. The thicknesses of the resulting 20 pressed electrodes were also measured with a step profiler. All nanoporous TiO_2 layers were annealed in air for 30 min at 500 °C. Figure 3 gives an overview of the investigated samples.

Photocurrent transients were excited with pulses of a N_2 laser (337 nm, 5 ns, repetition rate 1 Hz). A logarithmic measurement system was based on a 100 MHz card (Gage, 100 Ms/s, 14 bit resolution, 10^8 samples) and on a logarithmic readout (800 points per pulse) with a logarithmic increment of averaging over neighbored data points. For photocurrent measurements, the electrodes were deposited into a 0.5M NaCl electrolyte (pH=2). As a remark, the carrier lifetime is determined by capture of excess electrons from TiO_2 nanoparticles into the electrolyte. Illumination was performed from the electrolyte side. The SnO_2:F back contact was connected to the ground. The measurement resistance

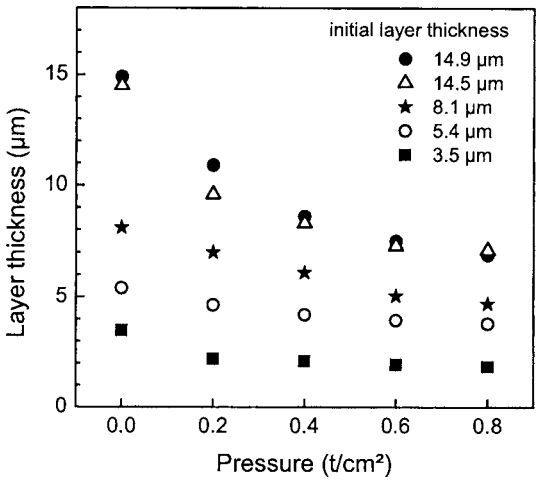

FIG. 3. Overview of the thicknesses and pressures of the investigated samples.

was 50 Ω. The peak time and the charge integrated over the photocurrent transients were analyzed as the main parameters.

PERCOLATION

The archetypal site-percolation model in three dimensions is a simple cubic lattice, where each site is occupied randomly with probability x or is empty with probability $c=1-x$. If the occupied sites are electrical conductors and the empty sites are insulators, the mixture is an insulator at low x values, while at large x values, many conducting paths between opposite edges of the sample exist, and the mixture is a conductor. A threshold concentration x_c exists where current can percolate across the sample, and it is called the percolation threshold or the critical concentration.

The percolation transition from insulator to conductor is a geometrical phase transition, which is characterized by the geometric properties of large clusters of nearest-neighbor sites in the neighborhood of x_c.[25] The probability X_∞ that a site belongs to the infinite cluster is 0 below x_c and increases above x_c as

$$X_\infty \propto (x-x_c)^\beta. \tag{4}$$

The dc conductivity of such a percolation system appears at the concentration x_c. If the electrical bonds between nearest-neighbor sites and their conductances are uniform, in the vicinity of x_c, the bulk conductivity also follows a power law equation,

$$\sigma_{\mathrm{dc}} = \sigma_a (x-x_c)^t, \tag{5}$$

where σ_a is a prefactor. Equation (5) is obtained in the theory of percolation in random resistor networks (RRNs),[26] i.e., a network of resistors in which a fraction of resistors has been removed at random. The exponents β and t are universal ($\beta=\beta_0=0.417$, $t=t_0=1.99$) for all three-dimensional (3D) lattices. This situation holds true even if the site conductivities have a distribution centered around some mean value. Contrarily, x_c depends on microscopic details of the lattice. In a 3D cubic lattice $x_c=0.25$. In this work, we compare the experimental result with site-percolation models. The reason

for this is that the electronic conductivity of TiO_2 nanoparticulate networks is mainly governed by electron transport in the bulk semiconductor material and not by particle interconnections.

The diffusion coefficient is related to dc conductivity by the Nernst-Einstein relation

$$D = \frac{k_B T \chi_n}{q^2 n_c} \sigma_{\mathrm{dc}}, \tag{6}$$

where n_c is the density of carriers, $k_B T$ is the thermal energy, q is the charge of the diffusing particles, and χ_n is a thermodynamic factor.[11] Long range conduction takes place through networks of connected particles. If the carriers are placed at random in the lattice, some of the carriers are placed in conducting regions that are totally enclosed by nonconducting regions. Since only carriers on the infinite cluster contribute to dc conductivity, we have from Eq. (4) $n \propto X_\infty \propto (x - x_c)^\beta$ and, therefore, the standard relationship obtained for the diffusion coefficient near and above the critical concentration takes the form[27]

$$D = D_a (x - x_c)^\delta, \tag{7}$$

where D_a is a prefactor and $\delta = t\text{-}\beta$, being $\delta = 1.58$ for the simple cubic lattice. However, in the transient photocurrent measurements reported here, the carriers photogenerated at one edge of the sample travel only through the connected regions. In addition, in the random walk simulations of Ref. 15, electrons were placed only in the infinite cluster. Therefore, in the discussions of the results below, it is justified to consider the carrier density and χ_n as constant factors so that geometrical variation of the diffusion coefficient is proportional to that of the conductivity.

It should be remarked that the power law expressions of the type (5) are rigorously derived by scaling methods but their validity is restricted to the low concentration x regime close to x_c. On the other hand, analytical description can be obtained also in the opposite limit of $c \approx 0$, i.e., when the fraction of missing sites is low, by using effective medium theories. This is a general method to calculate the average properties of disordered systems by a suitably determined homogeneous effective medium. The value for a simple, representative element of the disordered system, embedded in the effective medium, is determined self-consistently. It is well established[23] that the EMA gives good results (in comparison with Monte Carlo simulation) of the behavior of the conductivity of a RRN $\sigma(x)$ when x is large, approaching the maximum $x = 1$. The normalized conductivity in simple EMA models has the form

$$\sigma_u(c) = \frac{\sigma}{\sigma_0} = [1 - 2\beta c + \gamma c^2], \tag{8}$$

where σ_0 is the conductivity at $c = 0$, and β and γ are constants that differ according to the method of calculation. The theory of Izyumov[28] and Kirkpatrick[26] provides the values

$$\beta = 1.260, \quad \gamma = 2\beta - 1 = 1.520, \tag{9}$$

and the theory of Bernasconi and Wiesmann gives[29]

$$\beta = \gamma = 1.2656. \tag{10}$$

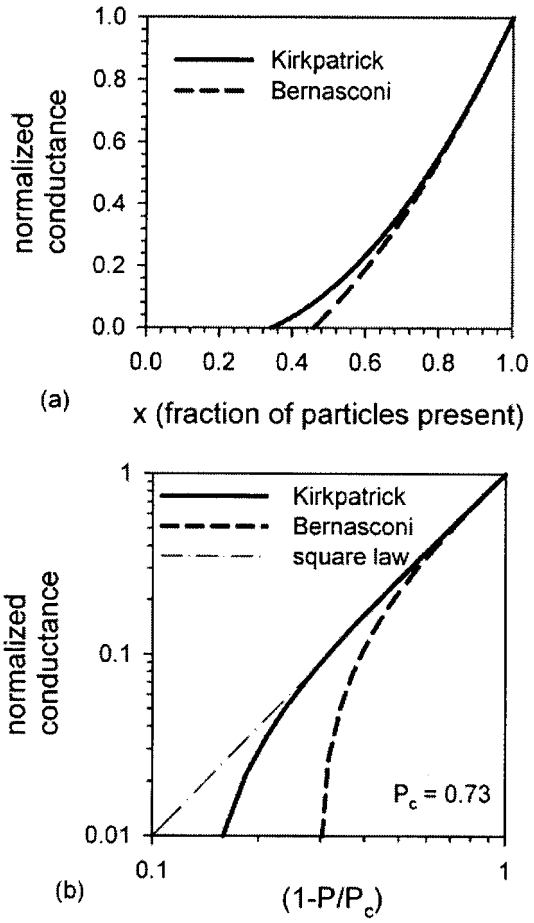

FIG. 4. Izyumov-Kirkpatrick (Refs. 26 and 28) and Bernasconi-Wiesmann (Ref. 29) analytical models of percolation conductivity for a 3D cubic lattice, in terms of (a) fractional occupation and (b) porosity of the lattice. The straight line indicates the dependence $(1 - P/P_c)^2$.

For the derivation of Eqs. (8)–(10), we refer to the original publications.[26,29] These models are represented in Fig. 4(a). It is observed in Eq. (8) that the conductivity is well described by a second order polynomial when x is large. Other versions of EMA formalism have been successfully used to model the effective diffusion coefficient in a variety of bidisperse media (see, for example, Ref. 30).

While percolation theories are usually cast in terms of a lattice occupation, parameter x, in the discussion of experimental results of pressed electrodes, the porosity P is the most convenient parameter, since the porosity is readily related to the film thickness. On the basis of a simple relationship $P = 1 - x$, the universal law near the threshold concentration takes the form

$$D = D_b |P - P_c|^n, \tag{11}$$

where D_b is a prefactor and P_c is the critical porosity. Equation (11) has been applied in previous works on nanostructured TiO_2 electrodes.[15,19] In these experimental works, exponents ranging between $n = 0.85$ and 2 were obtained, and the value $P_c = 0.76$ has provided a good description of the results in all the cases. For later reference, it is important to note that the Izyumov-Kirkpatrick[26,28] and Bernasconi-Wiesmann[29] theories show a good agreement

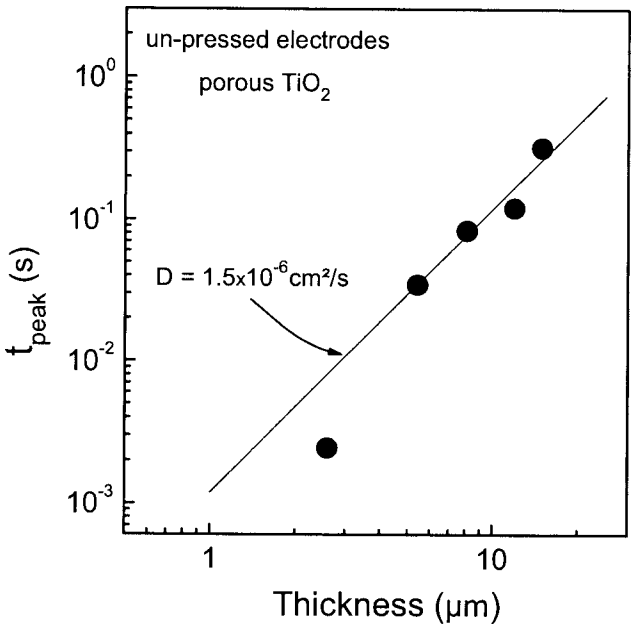

FIG. 5. Dependence of t_{peak} on the layer thickness of unpressed electrodes. The solid line gives the dependence for $D=1.5\times10^{-6}$ cm^2/s.

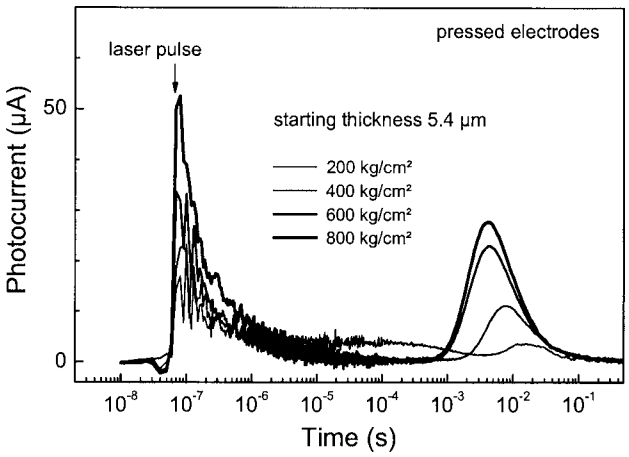

FIG. 6. Photocurrent transients of pressed porous TiO_2 electrodes with initial layer thickness of 5.4 μm.

with Eq. (11) at *low porosity*, provided that $n\approx2$, which is the universal value for regular 3D lattices [see Fig. 4(b)].

The porosity of a network of randomly packed spheres cannot be directly identified with a probability of lattice occupation because even at the maximum packing densities obtained, the void fraction is ≈0.35. We have proposed in the Appendix a simple approximate procedure of conversion between occupation and porosity. We should remark that such procedure is arbitrary to some extent and is used here as a pragmatic tool in order to compare the experimental data with the percolation conductivity theories.

In summary, EMA methods provide an estimate of the conductivity over a wide range of porosity, but they are not accurate near x_c. Renormalization group methods[31] provide a more accurate description of the transport properties near x_c, but the computations are quite complex. Therefore, analytical descriptions are not available over the entire range of porosities. Further detailed information about percolation in porous media can be found in the textbook.[23]

RESULTS AND DISCUSSION

Figure 5 shows the dependence of the photocurrent peak time t_{peak} on the layer thickness for the unpressed electrodes. For the larger thicknesses, this dependence follows very well a power law with the power coefficient of 2. Therefore, a diffusion coefficient following Eq. (2) can be obtained (about 1.5×10^{-6} cm^2/s).

Some typical photocurrent transients are shown in Fig. 6 for pressed nanoporous TiO_2 electrodes (initial thickness of 5.4 μm). As can be seen, the value of t_{peak} shifts toward shorter times with increasing pressure, i.e., decreasing layer thickness.

With respect to the interpretation of the photocurrent transients, we should point out some essential differences with respect to standard time-of-flight (TOF) technique in compact semiconductors. The photocurrent transients in porous TiO_2 surrounded with electrolyte have been pioneered by Solbrand *et al.*[32] For illumination from the electrolyte side, the transients are characterized by a peak shape related to the diffusion coefficient as indicated in Eq. (2) and Fig. 6, in contrast to classic TOF signal, which decays from the beginning. The reason for this was clarified in Ref. 33: the current transient measured in the external circuit reflects the arrival of electrons at the collecting substrate and not the movement of charges in the TiO_2 (displacement current). Recently, transient photocurrent peaks have been described in full detail[20] using numerical models that allow us to treat the recombination phenomena coupled with diffusion.

Another aspect worth discussing is the possible appearance of dispersive transport that will affect the determination of effective diffusion coefficient. Electron transport in nanostructured TiO_2 is usually well described by a multiple trapping model with an exponential distribution. Such distribution indeed provides dispersive transport in TOF measurements of amorphous semiconductors.[34] On the other hand, steady-state measurements of electron diffusion in DSC in the frequency domain by small perturbation methods do not show indication of dispersive transport.[35] The reason for this is that transient photocurrent peaks occur in a time scale where all the electron distribution is thermalized in traps,[33] and this is aided in the experiments described in the present work by the repetition of the pulses at 1 Hz, which causes a certain steady-state to be established in the sample. The recent paper by Van de Lagemaat *et al.*[36] shows the temporal evolution of the diffusion coefficient in porous TiO_2: dispersive transport appears at times shorter than 1 ms, while at longer times, the diffusion coefficient becomes constant. Therefore, it can be considered that the photocurrent transient peaks in the present work can be well described by ordinary diffusion model, by opposition to dispersive or anomalous diffusion, which appears at much shorter time scales.[37,38]

The dependence of t_{peak} on the layer thickness of the pressed electrodes is given in Fig. 7 for the layers with different initial thicknesses. Similarly as for the unpressed electrodes, the electrodes pressed at 200 kg/cm^2 follow a power

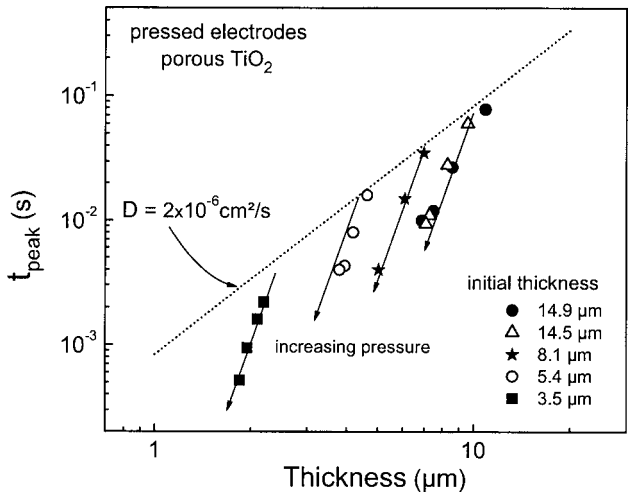

FIG. 7. Dependence of t_{peak} on the layer thickness for pressed electrodes with different initial thicknesses. The pressures were 0.2, 0.4, 0.6, and 0.8 t/cm^2. The dotted line gives the dependence for $D=2\times10^{-6}$ cm^2/s.

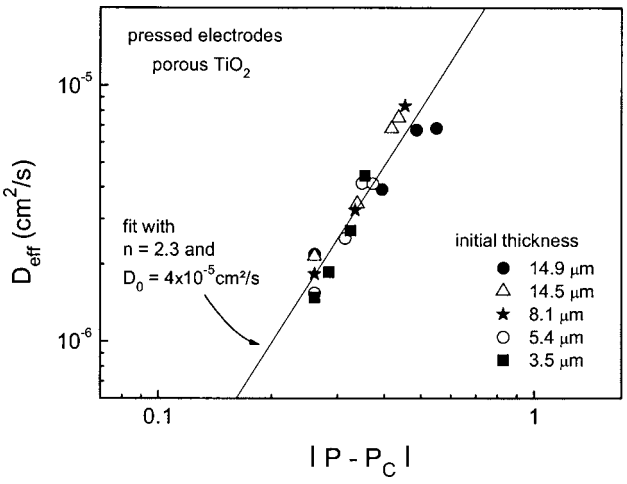

FIG. 9. Dependence of D_{eff} on the porosity of the pressed porous TiO_2 electrodes for the different initial thicknesses. P_C is the critical porosity (0.76). The solid line shows the slope of 2.3.

law with the power coefficient of 2 ($D=2\times10^{-6}$ cm^2/s). However, within each series with the same initial thickness, t_{peak} decreases much stronger than expected from simple diffusion (power coefficient much larger than 2). Therefore, the diffusion coefficient changes within each series of the same initial layer thickness.

The dependence of the charge of the integrated photocurrent transients on t_{peak} is depicted in Fig. 8(a). The charge decreases with increasing t_{peak} for t_{peak} larger than 10 ms. From theoretical analysis, it is known that the charge decreases by about one order of magnitude if the carrier lifetime is equal to $t_{peak}{}^0$ ($t_{peak}{}^0$ is t_{peak} in the case of carrier lifetimes significantly longer than t_{peak}, i.e., when the diffusion peak of the transient photocurrent is not affected by the decrease of the number of carriers by recombination). The carrier lifetime is about 100 ms for the given experimental configuration, i.e., sintered TiO_2 nanoparticles in aqueous NaCl solution (pH=2). Therefore, it is reasonable to consider undisturbed values of t_{peak} for the given experiments.

In a first stage of analysis of the data, regarding to percolation theory, the effective diffusion coefficient D_{eff} should depend on $|P-P_c|$ by a universal law. The effective layer thickness (L_{eff}) for diffusion is less than the layer thickness measured by the step profiler due to the absorption length (α^{-1}) and its scaling with the porosity. The dependence of the effective layer thickness on α^{-1} and P has been considered by the following equation, which takes into account the change of the absorption coefficient due to the increase of TiO_2 per film thickness,

$$L_{eff}=L-\frac{\alpha^{-1}}{1-P}. \tag{12}$$

Therefore, the effective diffusion coefficient is given by

$$D_{eff}=\frac{L_{eff}{}^2}{6t_{peak}}. \tag{13}$$

The porosity of the layers scales with the change of the layer thickness after pressing. For simplicity, a constant porosity is assumed for the layers pressed at 200 kg/cm^2 (P'). This assumption is reasonable since the layers pressed at 200 kg/cm^2 are characterized by nearly the same diffusion coefficient. The thicknesses of the layers pressed at 200 kg/cm^2 are denoted by L'. As explained before, the nanoparticles are incompressible; hence, the pressing decreases the void space and, therefore, the porosities of the pressed electrodes (porosity P, layer thickness L) are given by the following expression:

$$P=\frac{L-(1-P')L'}{L}. \tag{14}$$

The data given in Fig. 7 can be fitted to one universal master plot (Fig. 9) using the critical porosity value $P_c=0.76$ and only two free fit parameters (α^{-1} and P'). The best fit was obtained for $\alpha^{-1}=0.4$ μm and $P'=0.45$.

The value of α^{-1} is significantly larger than the reciprocal absorption coefficient of compact TiO_2 (about 0.1 μm at wavelength of 337 nm).[39] For porous TiO_2, the penetration of light will be larger with respect to the porosity. The roughness of the interface of the porous TiO_2 layer with the bulk electrolyte can also influence the effective penetration of light with respect to the diffusion of photoelectrons.

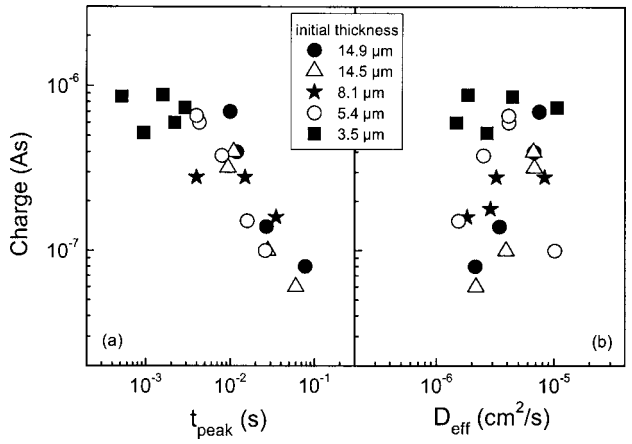

FIG. 8. Dependence of the charge integrated over the diffusion peak on (a) t_{peak} and (b) D_{eff}.

TABLE I. Diffusion coefficient in Monte Carlo simulation (Ref. 15) as a function of porosity converted into a fractional occupancy x.

Porosity	x	D	Normalized D
0.750 756	0.527 254	0.048 713	0.057 402
0.725 893	0.563 600	0.094 216	0.111 022
0.701 042	0.598 562	0.150 186	0.176 976
0.676 204	0.632 283	0.190 373	0.224 331
0.651 377	0.664 889	0.248 747	0.293 117

The value of P' is in excellent agreement with absorption measurements of dye molecules adsorbed on the internal surface of the porous TiO_2. The dependence of D_{eff} on $|P-P_c|$ can be expressed by Eq. (11) with $D_b=4\times10^{-5}$ cm^2/s for $n=2.3$. We remark that the power coefficient is generally about 2 for pressed TiO_2 electrodes. The values of D_{eff} and, therefore, the value of D_{cb} depend sensitively on factors such as the deposition temperature during EPD.[16]

Figure 8(a) demonstrates also that the densities of photoelectrons can be different for different measurements. It is well-known that the photoelectron density can significantly influence the effective diffusion coefficient of porous semiconductors, in general. However, we could not find any correlation between the integrated charge and the value of D_{eff} [fig. 8(b)]. Therefore, the observed differences of D_{eff} are related to geometrical changes in the porous TiO_2 layers due to pressing.

The preceding analysis is in general agreement with previous results[15,19] that were obtained for more restricted set of data. Therefore, it appears that the diffusion coefficient of TiO_2 electrodes with variable porosity is well adapted to the universal law of Eq. (11). However, it is also interesting to consider what is the span of the data in the general variation of the percolation conductivity, which is outlined in Fig. 4(a) for simple EMA theories. In fact, Eq. (11) is only justified if $|P-P_c|$ is small; however, under the heavy pressing applied in the samples, it appears that the porosity should be significantly reduced with respect to the critical value. Furthermore, as mentioned before, although the value $P_c=0.76$ is stable in different experiments, large differences of the exponent n have been observed.

In order to consider these questions, we have carried out an additional analysis that consists in converting the porosity to lattice occupancy as described in the Appendix. While this procedure is approximate at best, it allows us to estimate the trends of the data in comparison with EMA theories that are best suited at low porosity values.

First, we have treated the results of Monte Carlo simulation obtained in Ref. 15. These data were kindly supplied by Van de Lagemaat. We have converted the reported porosities into a fractional occupancy x and the values are listed in Table I. The results have been fitted to an expression of the type (7). Equation (7) allows us to determine a normalized diffusion coefficient with respect to the value at $x=1$, assuming that such variation law is valid in the whole range of $x>x_c$. The normalized diffusion coefficient, thus, obtained is shown in Fig. 10. A similar analysis has been performed with

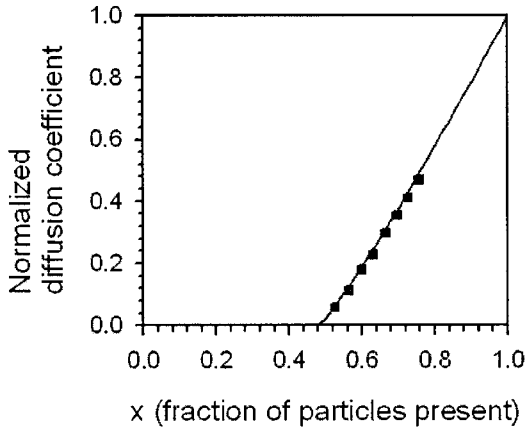

FIG. 10. Plot of the numerical results obtained by random walk simulation in Ref. 15 as a function of lattice occupancy. The fit to Eq. (7) gives $D_a=1.864\,877$, $\delta=1.201\,378$, and $x_c=0.479\,128$. The diffusion coefficient has been normalized to the value at $x=1$ obtained from the fit.

a set of data for films of different initial thicknesses that were previously given in Fig. 9. Such data have been fitted to the EMA expression,

$$D(c)=D_c[1-2\beta c+\gamma c^2], \tag{15}$$

where D_c is a prefactor. These results as well as those of Fig. 10 have been plotted together in Fig. 11, where the predictions of EMA theories are also shown. It must be remarked that no assumption about the critical value x_c is imposed in the fits of Fig. 11. Therefore, the fact that the different sets of data agree with each other and also fall close to the Bernasconi-Wiesmann[29] model (which is more accurate than the Izyumov-Kirkpatrick[26,28] model) strongly supports the application of the percolation theory to nanoporous TiO_2

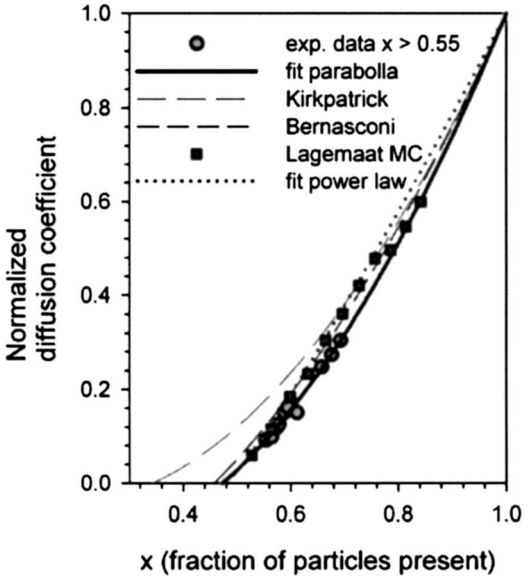

FIG. 11. Representation of normalized diffusion coefficient as a function of fractional occupation of the lattice. Shown are the Izyumov-Kirkpatrick (Refs. 26 and 28) and Bernasconi-Wiesmann (Ref. 29) percolation theories, the data of Fig. 8 for $x>0.55$ (except those of $L=14.9$ μm), the numerical data obtained by random walk simulation in Ref. 15, and parabollic fits to the two sets of data following Eq. (15). The diffusion coefficient has been normalized in all cases to the value at $x=1$ obtained from the fits.

films of different thicknesses. It should be observed that the data can be well described alternatively by laws [Eq. (7) and (15)]. However, we have indicated in Fig. 4(b) that the universal power law also agrees with the EMA models in the regime of very low porosity. By placing the data on a common plot (Fig. 11), it is observed that our experimental data show a very similar behavior to the results of Monte Carlo simulation, even if the power law exponents gave very different results. Therefore, we must conclude that the power law exponent is very sensitive to the experimental errors in the data.

CONCLUSION

In this work, we have analyzed the dependence of the electron diffusion coefficient on the porosity in a variety of samples and it was shown that the variation can be well described by percolation theory. A combination of power law dependence and EMA models indicates that the accessible geometries are situated in an intermediate regime between the percolation threshold and the unbroken lattice. The internal connectivity of the nanoparticulate network, therefore, has an important influence over the rate of electron diffusion and constitutes an important factor determining the quality of nanoparticulate films formed by wet chemical methods and eventually in the performance of devices.

ACKNOWLEDGMENTS

The work was supported by Ministerio de Educación y Ciencia of Spain under Project Nos. MAT2007-62982 and HOPE CSD2007-00007 (Consolider-Ingenio 2010) (J.B.) and the Israeli Ministry of Science (the BIU group).

APPENDIX: POROSITY AND FRACTIONAL OCCUPANCY OF A DISORDERED LATTICE

The porosity is defined by the ratio $P=V_p/V_m$, where V_p is the nonsolid volume and V_m is the total volume of material, including the solid and nonsolid parts. The packing fraction ϕ of a regular packing of spheres is the fraction of a volume filled by the spheres, $\phi=1-P$. The densest possible packing fraction is 0.7405 corresponding to the close-packed face-centered cubic (fcc) lattice.[40] For simple cubic regular lattice with coordination number $N=6$, it is $\phi=0.52$, and $\phi=0.3401$ in tetrahedral lattice packing in which each sphere touches four neighbors. Random close packing of spheres gives packing densities in the range of 0.06–0.65.[40] Computer simulations of disordered nanoparticulate networks showed that the coordination numbers of random packed structures with different porosities follow loosely the tendency for the regular structures.[14] The following approximate relationship was derived for disordered structures:

$$N=\frac{3.08}{P}-1.13. \tag{A1}$$

In a random network of equally sized randomly packaged spheres, the notion of occupation of lattice sites is not well-defined and the determination of percolation thresholds requires special criteria.[41] We shall represent the randomly arranged sphere packing of TiO_2 nanoparticles as a regular lattice with spheres present with a probability x, i.e., with a fraction $c=1-x$ of spheres missing in random sites of the lattice. The fractional void volume of a nanoparticulate film must be divided into the fraction c of empty lattice sites and the void volume in the unit cell of occupied sites, $(1-\phi)x$,

$$P=c+(1-\phi)x=1-\phi x. \tag{A2}$$

In a random package of spheres, this division is to some extent arbitrary. The fraction of empty sites, c, is related to the number of pores of size larger than the spheres. For describing consecutively pressed TiO_2 films, we must take into account that the packing fraction ϕ increases with increasing x because the structure becomes more tightly packaged, as well as less defective, when the film is compressed. We will assume a linear relation

$$\phi(x)=A+Bx. \tag{A3}$$

Here, $A=\phi_1-Bx_1$ and $B=(\phi_2-\phi_1)/(x_2-x_1)$, in terms of two reference values of ϕ and x. The porosity provides an occupation probability as follows:

$$x=\frac{[A^2+4B(1-P)]^{1/2}-A}{2B}. \tag{A4}$$

Random networks of spheres with porosity of about 0.5 have a coordination number between 6 and 5 that corresponds most closely to the simple cubic lattice. The simple cubic lattice with $\phi=0.52$ has been the most investigated in simulations and describes most correctly the practical porosities investigated. Furthermore, it was found that networks of randomly packaged spheres with packing density $\phi=0.6$ have the same critical size concentration, $x_c=0.32$, as the simple cubic lattice.[41] In order to match the coordination numbers as a function of porosity reported in Ref. 14, we assume the reference values indicated in Table II, where also the resulting porosities from Eq. (A2) are indicated. From

TABLE II. Parameters selected for relating porosity with a lattice occupancy.

Lattice occupancy	Packing fraction	Porosity
$x_1=0.6$	$\phi_1=0.5$	$P_1=0.7$
$x_2=1$	$\phi_2=0.65$	$P_2=0.35$

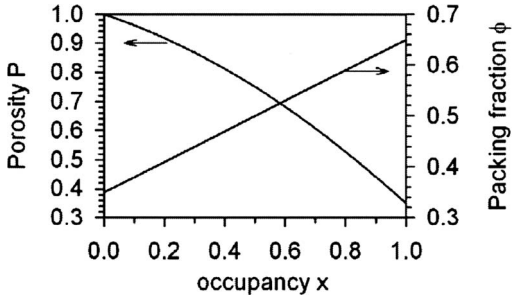

FIG. 12. Assumed relationship between porosity, packing fraction, and occupancy according to parameters in Table I.

these values, the parameters used for the conversion of lattice occupancy to porosity ($A=0.35$, $B=0.30$) are obtained, and they are indicated in Fig. 12).

[1] B. O'Regan and M. Grätzel, Nature (London) **353**, 737 (1991).
[2] C. Bechinger, S. Ferrer, A. Zaban, J. Sprague, and B. A. Gregg, Nature (London) **383**, 608 (1996).
[3] R. Cinnsealach, G. Boschloo, S. N. Rao, and D. Fitzmaurice, Sol. Energy Mater. Sol. Cells **57**, 107 (1999).
[4] E. Topoglidis, E. Palomares, Y. Astuti, A. Green, C. J. Campbell, and J. R. Durrant, Electroanalysis **17**, 1035 (2005).
[5] E. A. Meulenkamp, J. Phys. Chem. B **103**, 7831 (1999).
[6] A. C. Fisher, L. M. Peter, E. A. Ponomarev, A. B. Walker, and K. G. U. Wijayantha, J. Phys. Chem. B **104**, 949 (2000).
[7] R. Könenkamp, Phys. Rev. B **61**, 11057 (2000).
[8] J. Van de Lagemaat and A. J. Frank, J. Phys. Chem. B **104**, 4292 (2000).
[9] I. Abayev, A. Zaban, F. Fabregat–Santiago, and J. Bisquert, Phys. Status Solidi A **196**, R4 (2003).
[10] A. Solbrand, H. Lindström, H. Rensmo, A. Hagfeldt, S. E. Lindquist, and S. Södergren, J. Phys. Chem. B **101**, 2514 (1997).
[11] J. Bisquert, Phys. Chem. Chem. Phys. **10**, 49 (2008).
[12] L. M. Peter, J. Phys. Chem. C **111**, 6601 (2007).
[13] J. Bisquert, J. Phys. Chem. B **108**, 2323 (2004).
[14] J. Van de Lagemaat, K. D. Benkstein, and A. J. Frank, J. Phys. Chem. B **105**, 12433 (2001).
[15] K. D. Benkstein, N. Kopidakis, J. Van de Lagemaat, and A. J. Frank, J. Phys. Chem. B **107**, 7759 (2003).
[16] S. Tirosh, T. Dittrich, A. Ofir, L. Grinis, and A. Zaban, J. Phys. Chem. B **110**, 16165 (2006).
[17] M. J. Cass, F. L. Qiu, A. B. Walker, A. C. Fisher, and L. M. Peter, J. Phys. Chem. B **107**, 113 (2003).
[18] M. Ni, M. K. H. Leung, D. Y. C. Leung, and K. Sumathy, Sol. Energy Mater. Sol. Cells **90**, 1331 (2006).
[19] T. Dittrich, A. Ofir, S. Tirosh, L. Grinis, and A. Zaban, Appl. Phys. Lett. **88**, 182110 (2006).
[20] S. Rühle and T. Dittrich, J. Phys. Chem. B **110**, 3883 (2006).
[21] N. Kopidakis, K. D. Benkstein, J. Van de Lagemaat, and A. J. Frank, J. Phys. Chem. B **107**, 11307 (2003).
[22] G. K. Mor, O. K. Varghese, M. Paulose, K. Shankar, and C. A. Grimes, Sol. Energy Mater. Sol. Cells **90**, 2011 (2006).
[23] M. Sahimi, *Applications of Percolation Theory* (CRC, Boca Raton, 1994).
[24] A. Ofir, T. Dittrich, S. Tirosh, L. Grinis, and A. Zaban, J. Appl. Phys. **100**, 074317 (2006).
[25] A. Bunde and J. W. Kantelhardt, *Diffusion in Condensed Matter*, 2nd ed., edited by J. Kärger and R. Haberlandt (Springer-Verlag, Berlin, 2005).
[26] S. Kirkpatrick, Rev. Mod. Phys. **45**, 574 (1973).
[27] J. Tobochnik, D. Laing, and G. Wilson, Phys. Rev. A **41**, 3052 (1990).
[28] Y. Izyumov, Proc. Phys. Soc. London **87**, 505 (1966).
[29] J. Bernasconi and H. J. Wiesmann, Phys. Rev. B **13**, 1131 (1976).
[30] J. Benzoni and H.-C. Chang, Chem. Eng. Sci. **39**, 161 (1983).
[31] M. Sahimi, B. D. Hughes, L. E. Scriven, and H. T. Davis, Phys. Rev. B **28**, 307 (1983).
[32] A. Solbrand, A. Henningsson, S. Sodergren, H. Lindstrom, A. Hagfeldt, and S.-E. Lindquist, J. Phys. Chem. B **103**, 1078 (1999).
[33] J. Van de Lagemaat and A. J. Frank, J. Phys. Chem. B **105**, 11194 (2001).
[34] T. Tiedje and A. Rose, Solid State Commun. **37**, 49 (1981).
[35] Q. Wang, S. Ito, M. Grätzel, F. Fabregat–Santiago, I. Mora–Seró, J. Bisquert, T. Bosshoa, and H. Imaic, J. Phys. Chem. B **110**, 19406 (2006).
[36] J. Van de Lagemaat, K. Zhu, K. D. Benkstein, and A. J. Frank, Inorg. Chim. Acta **620**, 361 (2008).
[37] T. Dittrich, I. Mora–Seró, G. Garcia–Belmonte, and J. Bisquert, Phys. Rev. B **73**, 045407 (2006).
[38] J. A. Anta, I. Mora–Seró, T. Dittrich, and J. Bisquert, J. Phys. Chem. C **111**, 13997 (2007).
[39] P. Chrysicopolou, D. Davazoglou, C. Trapalis, and G. Kordas, Thin Solid Films **323**, 188 (1988).
[40] S. Torquato, T. M. Truskett, and P. G. Debenedetti, Phys. Rev. Lett. **84**, 2064 (2000).
[41] M. Ahmadzadeh and A. W. Simpson, Phys. Rev. B **25**, 4633 (1982).